Heliyon 10 (2024) e33025

Contents lists available at ScienceDirect

Heliyon

journal homepage: www.cell.com/heliyon

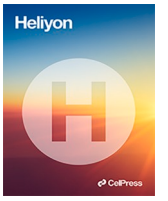

Research article

A flexible and dissolving traditional Chinese medicine microneedle patch for sleep-aid intervention

Chunhua He [a], Zewen Fang [a], Heng Wu [b,*], Xiaoping Li [a,**], Lianglun Cheng [a], Yangxing Wen [c,***], Juze Lin [d]

[a] School of Computer, Guangdong University of Technology, Guangzhou, 510006, Guangdong, PR China
[b] School of Automation, Guangdong University of Technology, Guangzhou, 510006, Guangdong, PR China
[c] First Affiliated Hospital, Sun Yat-Sen University, Guangzhou, 510080, Guangdong, PR China
[d] Guangdong Provincial People's Hospital, Guangzhou, 510000, Guangdong, PR China

ARTICLE INFO

Index terms:
Dissolving microneedle patch
Traditional Chinese medicine
Sleep aid
EEG signal
Flexible material

ABSTRACT

About a quarter of the world's population suffers from insomnia, and the number of the insomniacs is gradually increasing. However, the current drug therapy and non-drug therapy sleep-aid methods have certain limitations. In general, the sleep-aid effect of drug therapy is better than that of Non-drug therapy, but western medicine may lead to some side effects and drug abuse. Although the side effects of Chinese Herbal Medicine (CHM) are relatively small, making the herbal decoction is complex and time-consuming. Therefore, exploring a novel sleep-aid method is very significant. In this paper, a flexible and dissolving Traditional Chinese Medicine (TCM) microneedle patch is proposed for sleep-aid intervention. The TCM microneedle patch is a micrometer-scale intrusive object, and the herbal extracts are carried by the patch. The materials, design method, and fabrication process of the microneedle patch have been described in detail. Besides, the mechanical characteristics of the microneedle patch, sleep-aid effect evaluation method, and experimental scheme have been presented. Three microneedle tips with radii of 5 μm, 15 μm, and 22 μm are selected for simulation analysis. Abaqus simulation results indicate that the smaller the radius of the microneedle tip, the smaller the piercing force. Considering that the microneedle should easily penetrate the skin without buckling, that is, the piercing force should be larger than the buckling force, thus 15 μm, instead of 5 μm or 22 μm, is more suitable to be adopted as the radius of the microneedle tip. For the microneedle with the radius of 15 μm, the piercing force is 0.033 N, and the difference between the piercing force and buckling force is 0.036 N. Experimental results demonstrate that the fracture force of the microneedle is about 0.29 N, which is far larger than the piercing force and buckling force. The single-lead EEG signals of the frontal lobe are used to evaluate the sleep-aid effect of the TCM microneedle patch. After sleep-aid intervention on the Anmian and Yintang acupoints using the patches, for most subjects, the ratios of the low-frequency brain wave energies to the high-frequency brain wave energies are increased obviously, indicating that the proposed sleep-aid method is effective.

* Corresponding author.
** Corresponding author.
*** Corresponding author.
E-mail addresses: heng.wu@foxmail.com (H. Wu), xpli@gdut.edu.cn (X. Li), wenyx5@mail.sysu.edu.cn (Y. Wen).

https://doi.org/10.1016/j.heliyon.2024.e33025
Received 3 March 2024; Received in revised form 12 June 2024; Accepted 12 June 2024
Available online 13 June 2024

1. Introduction

Insomnia is a common health problem worldwide, and becomes a heavy global burden. About a quarter of the world's population suffers from insomnia, and the number of the insomniacs is gradually increasing [1]. In recent decades, for most people, the sleep time has gradually decreased, and sleep quality is deteriorating. Insomnia poses significant challenges to public health. It is a common disease associated with marked impairment in function and quality of life, psychiatric and physical morbidity, and accidents [2]. Insomnia is an important risk factor for diabetes, heart disease, obesity and depression [3,4]. In addition, insomnia leads to low work efficiency, increased stress, and decreased quality of life [5,6]. Therefore, the relevant sleep-aid methods are more and more important.

The common treatment methods mainly include drug therapy and non-drug therapy. Drug therapy method for insomnia mainly includes Benzodiazepine Receptor Agonists (BZRAs) and Non-Benzodiazepine hypnotics (non-BZDs), antidepressants with hypnotic effects [7], antihistamines [8], melatonin receptor agonists [9], novel orexin receptor antagonists [10], and CHM. CHM has been proved to be effective for sleep aid intervention since it can make systematic adjustment for the insomniacs from the root. Ziziphus jujuba spinosa kernel (Suan Zao Ren), polygala tenuifolia (Yuan Zhi), schizandra chinensis (Wu Wei Zi), platycladus orientalis kernel (Bai Zi Ren) are commonly applied to treat insomnia [11]. Non-drug therapy method for insomnia mainly includes psychotherapy and physiotherapy. For psychotherapy, Cognitive Behavioral Therapy for Insomnia (CBTI) is widely adopted [12]. For physiotherapy, Non-invasive Brain Stimulation (NIBS), such as auditory stimulation [13], Transcranial Current Stimulation (TCS) [14] and Transcranial Magnetic Stimulation (TMS) [15], can regulate wakefulness and sleep through the cortical-hypothalamic top-down sleep-wake regulatory pathway [16]. Besides, acupuncture has been used to treat sleep problems since ancient times in China [17–19]. The sleep-aid acupoints used for acupuncture mainly comprise Yintang, Anmian, Shenting, Baihui, Shenmen, and Sanyinjiao [20–23].

However, the current methods all have limitations. Although acupuncture is very effective for sleep aid intervention, the traditional acupuncture method requires not only the high skill of applying acupuncture, but also rich experience to find the correct acupoint. In general, the sleep-aid effect of drug therapy is better than that of Non-drug therapy. Drug therapy methods are usually effective, but western medicine may lead to some side effects and drug abuse. Although the side effects of CHM are relatively small, making the herbal decoction is complex and time-consuming. Besides, drinking the herbal decoction is a painful experience. In general, the effect of a single sleep-aid method is limited, so the integration of multiple sleep-aid intervention methods is a trend. The above analysis indicates that CHM is a better drug therapy method, and acupoint acupuncture is a better non-drug therapy method. If they are combined, the sleep-aid effect will be better. However, their above shortcomings are very obvious and urgently need to be overcome. Therefore, exploring a new sleep-aid method is very significant.

In order to avoid the pain of traditional drug delivery and advance the drug absorption efficiency, recently, a novel drug delivery technique with microneedle (MN) patch has been proposed. For a long time, the skin has been considered an attractive drug delivery site because it avoids first-pass metabolism in the liver and enzymatic degradation in the gastrointestinal tract [24]. However, the Stratum Corneum (SC) of the skin limits the drug delivery. MN is a micrometer-scale intrusive object, which has four types: hollow, solid, dissolving and encapsulated [25]. Among them, dissolving MN (DMN) is the most commonly used and typically consists of biodegradable polymers, such as polyvinyl alcohol, polyvinylpyrrolidone, and Hyaluronic Acid (HA) [26]. After the MN penetrates the SC and reaches the dermis, the drugs gradually release from the encapsulated matrix [27], which greatly improves the convenience and efficiency of drug delivery [28]. Besides, the MN patch also has the effect of acupuncture. Because the patch is a MN array, it reduces the requirements for acupoint positioning and avoids the heavy dependence of traditional acupuncture on experience. Due to the high efficiency and painless experience of this innovative drug delivery technique, MN patches have been paid more and more attention.

In recent years, many studies have attempted to use the MN patch to treat insomnia. Qi et al. has developed a MN patch prepared from proline, melatonin and silk fibroin [29]. The in vivo experimental results of the Sprague Dawley (SD) rat indicated that the MN patch released the drug into the body through the skin and maintained a high concentration. Zhu et al. has reported a new formulation of the armodafinil MN patch [30]. After the treatment of sleep deprived mice with the MN patch, the in vivo pharmacodynamics study clearly demonstrated that the armodafinil MN patch could eliminate the influence of sleep deprivation. However, the previous work has limitations since the melatonin's effect on adults is limited [31] and armodafinil is an addictive prescription drug [32]. Similarly, using MN patch as the CHM carrier can be conveniently used to treat insomnia. Nowadays, there are a lot of studies on using the CHM MN patch to treat skin diseases [33,34], but few studies have been reported to treat insomnia.

On the other hand, the evaluation method of sleep aid effect is also very important. Compared to subjects with good sleep, the secretions of corticosteroids and adrenaline of subjects with poor sleep are increased. Subjects with sleep-onset insomnia have increased heart rate and finger temperature [35,36], and possess more beta wave energy and less alpha wave energy [37,38]. The power spectral densities of brain waves in insomnia subjects are higher during the whole sleep period, especially in the high-frequency band [39]. Hence, brain wave energies of the ElectroEncephaloGraphy (EEG) signal can be used to evaluate the sleep-aid effect. In the past, multi-lead EEG signals, such as 128 or 256 leads [40], were widely used for sleep quality evaluation. Although the evaluation results are very accurate, the evaluation process is very cumbersome. For example, electrode connection usually takes 1 h, and wearing multiple electrodes on the head makes the users uncomfortable, thus affecting the sleep quality. In recent years, some studies demonstrated that the accuracy of the sleep quality evaluation using the single-lead EEG signal from the prefrontal lobe was much approximate to that using the multi-lead EEG signals [41–43], which makes the single-lead EEG signal evaluation method increasingly popular.

Therefore, aiming at the issues and limitations of the existing sleep-aid methods mentioned above, this paper proposes a flexible and dissolving TCM microneedle patch to achieve better sleep-aid effect and comfortable experience. The materials, design method, fabrication process, and mechanical characteristics of the MN patch will be presented in detail, and the sleep-aid evaluation method with single-lead EEG signal is also put forward.

2. Materials and methods

2.1. Materials for microneedle patch

In this work, ziziphus jujuba spinosa kernel (Suan Zao Ren), polygala tenuifolia (Yuan Zhi), albizia julibrissin flower (He Huan Hua), polygonum multiflorum stem (Shou Wu Teng), schizandra chinensis (Wu Wei Zi), nelumbo nucifera seed (Lian Zi) and coptis chinensis (Huang Lian) are used as the TCM materials for the MN patch. Here, Suan Zao Ren is utilized to nourish the liver, calm the heart and nerves, and reduce the sweat [44]. Yuan Zhi is used to calm the nerves, promote the intelligence, dispel the phlegm, and reduce the swelling [45]. He Huan Hua is applied to treat restlessness, depression and insomnia [46]. Shou Wu Teng is utilized to nourish the heart, dispel the rheumatism, calm the nerves, and unblock the meridians [47]. Wu Wei Zi is used to moisturize the lung, nourish the kidney, generate saliva, stop cough, reduce the sweat [48]. Lian Zi is applied to nourish the spleen, tonify the kidney, stop the diarrhea, nourish the heart, and calm the nerves [49]. Both Wu Wei Zi and Lian Zi can promote the growth of sperm. Huang Lian is adopted to clear the heat, eliminate the inflammation, detoxify the body, stop the diarrhea, lower the blood glucose and lipid, and it is antibacterial and antiviral [50].

As a sleep-aid prescription, the masses of Suan Zao Ren, Yuan Zhi, He Huan Hua, Shou Wu Teng, Wu Wei Zi, Lian Zi and Huang Lian are set to 20 g, 13 g, 10 g, 30 g, 9 g, 12 g and 6 g respectively, with a total mass of 100 g. If the CHM compound is made into a herbal decoction, the process is time-consuming and drinking is also a painful experience. In addition, the drug ingredients absorbed into the blood circulation system through the stomach are very less, indicating a low efficiency of drug delivery. In fact, not all the ingredients in the herb are useful, some impurities such as lignin and moisture are useless. Thus, some impurities can be eliminated by purifying. The production process of the CHM related products mainly includes extraction, concentration, and drying. The active ingredients of these seven herbs can be extracted with alcohol, and the residue can be filtered effectively [44–50]. The resulting liquid is concentrated to remove excess water, and dried to obtain the powders.

The active ingredients of Suan Zao Ren include jujuboside A ($C_{58}H_{94}O_{26}$), jujuboside B ($C_{52}H_{84}O_{21}$), spinosin ($C_{28}H_{32}O_{15}$) and betulinic acid ($C_{30}H_{48}O_3$). The active ingredient of Yuan Zhi includes tenuifolin ($C_{36}H_{56}O_{12}$). The active ingredients of He Huan Hua include quercitrin ($C_{21}H_{20}O_{11}$) and linalool ($C_{10}H_{18}O$). The active ingredients of Shou Wu Teng include rheum emodin ($C_{15}H_{10}O_5$), rheinic acid ($C_{15}H_8O_6$), aloe-emodin ($C_{15}H_{10}O_5$), chrysophanol ($C_{15}H_{10}O_4$) and physcion ($C_{16}H_{12}O_5$). The active ingredient of Wu Wei Zi includes schisandrin ($C_{24}H_{32}O_7$). The active ingredient of Lian Zi is higenaminedl ($C_{16}H_{17}NO_3$). The active ingredient of Huang Lian is berberine ($C_{20}H_{17}NO_4$). Considering that the extraction of active ingredients requires multiple complex processes, such as soaking and decocting, adsorption and filtration, precipitation and separation, rotary evaporation, spray drying or freeze-drying, as illustrated in Fig. 1(a)~(d), the cost is very high and the yield is low. In addition, TCM emphasizes the systematic balance of yin and yang, as well as the roles of monarch and minister, assistant and guide. Although the active ingredients mentioned above play a key role, other minor ingredients can also play a certain auxiliary role. Therefore, there is no need to purify Chinese herbs as high as possible, just a simple extraction is needed to remove the useless ingredients.

On the other hand, Hyaluronic Acid (HA) is a glycosaminoglycan, and is an indigenous component of the connective tissues and dermis. It has high clinical value and has been widely used in various ophthalmic surgeries, such as lens implantation, anti-glaucoma surgery and corneal transplantation. It can also be applied to treat arthritis and accelerate wound healing. When used in cosmetics, it can keep the skin moist, smooth and elastic, with anti-wrinkle and whitening effects. It is dissolving in the skin and the degradation residues are very safe, making it highly suitable as a drug carrier. Therefore, this work will choose it as the carrier for the Chinese herbs.

Due to the mature application of DMN patches in the field of cosmetics, as well as the relatively complete processing technique and safety standards, this work will fabricate the TCM DMN patch based on cosmetic processing technique, instead of the medicine processing technique. Thus, according to the relevant requirements of the national laws and regulations, mandatory standards and technical specifications, only the ingredients listed in the Cosmetic Ingredients Catalog (CIC), International Nomenclature Cosmetic Ingredient (INCI) or International Cosmetic Ingredient Dictionary and Handbook (ICIDH) can be chosen. Owing to the fact that the extract of the Chinese herbal compound is not listed in those catalogs, only the extract of the individual herb can be selected as the raw material.

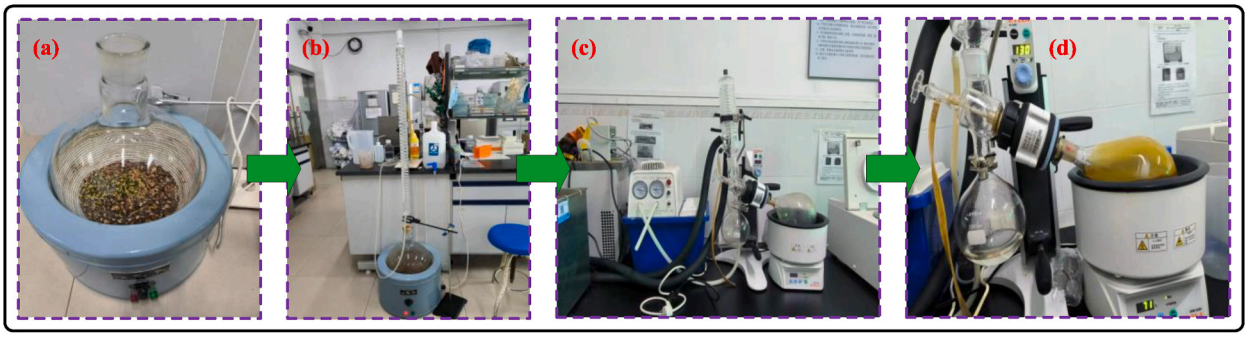

Fig. 1. a Soaking the Chinese herbs. **b** Decocting the Chinese herbs. **c** Performing adsorption and filtration, precipitation and separation. **d** Conducting rotary evaporation.

Considering standardization and safety, the extracts of Suan Zao Ren, Yuan Zhi, He Huan Hua, Shou Wu Teng, Wu Wei Zi, Lian Zi and Huang Lian are finished by EFONG Pharmaceutical Co., LTD (Foshan, Guangdong, China). For every herb, the reports of Material Safety Data Sheet (MSDS) and Certificate of Analysis (COA) are offered by the third-party testing and certification agency. The paste rates and yield rates of the extracts of the Chinese herbs are listed in Table 1. The paste rate refers to the ratio of the mass of active ingredients extracted from the herb to the raw mass of the herb. The yield rate refers to the ratio of the sum of the mass of active ingredients extracted from the herb and the mass of the dextrin impurity, to the raw mass of the herb. The current extraction process requires the addition of dextrin, and the amount of dextrin varies with the herb, as shown in Table 1. When dextrin is not considered, the mass ratios of the 7 herbal extracts of the TCM prescription are set to 20 %, 13 %, 10 %, 30 %, 9 %, 12 %, and 6 %, respectively. However, when dextrin is considered, the mass ratios of the 7 herbal extracts of the TCM prescription should be adjusted to 19.6 %, 12.3 %, 8.7 %, 29.1 %, 10.4 %, 14.3 % and 5.6 %, respectively. Thus, the mass of every herbal extract can be finally confirmed by the total extracts mass. For instance, if the mass of the total extracts is 100 g, the masses of the 7 herbs are 19.6 g, 12.3 g, 8.7 g, 29.1 g, 10.4 g, 14.3 g and 5.6 g, respectively.

2.2. Design and fabrication

Skin is the largest immune organ of the human body, mainly composed of three parts: the epidermis, dermis and hypodermis, as illustrated in Fig. 2a. The epidermis can be further divided into the stratum corneum, stratum lucidum, stratum granulosum, stratum spinosum and stratum basale. The stratum corneum is a brick wall structure with protective and waterproof functions, and its thickness is usually 10–20 μm. The stratum lucidum can control the skin's moisture, and prevent a large amount of water loss and inflow. The stratum granulosum can prevent the foreign objects from invading and filter the ultraviolet rays. The stratum spinosum can transport nutrients and repair damage. The basal layer has a strong ability for cell division and reproduction.

The total thickness of the epidermis is 50∼150 μm, while that of the dermis is 1∼4 mm. The dermis is a complex tissue composed of collagen fibers, elastic fibers, blood vessels, nerves and glands. The papillar region is mainly composed of collagen fibers and elastic fibers, making the skin elastic. In addition, the reticular region contains a large number of capillaries and lymphatic vessels. It provides oxygen and nutrients to the skin, helps to maintain normal metabolic activity, and facilitates the diffusion of drugs in the tissues. The hypodermis includes adipose tissue, connective tissue, and lymphatic tissue, with a thickness greater than 1 mm. Adipose tissue can absorb and disperse external shocks, reducing the risk of skin damage. Connective tissue can maintain the elasticity of the skin. Lymphatic tissue can help the body fight against infections and diseases.

Given that the stratum corneum has a certain blocking effect on drugs penetration, while the dermis can facilitate the diffusion of drugs, therefore the microneedle should penetrate the epidermis and reach the dermis for drug delivery, as shown in Fig. 2b. For facilitating penetration into the skin and increasing the drug loading, the microneedle adopts the shape of a bullet head. The finished product of the TCM DMN patch is depicted in Fig. 2c. The diameter of every patch is set to 1.7 cm and the diameter of the DMN array is about 1.2 cm, thus the corresponding area is large enough to cover the whole acupoint. The DMN array is mounted on the tape base. The physical picture of the TCM DMN patch is depicted in Fig. 2d, and the enlarged view of the DMN patch obtained by the microscope is illustrated in Fig. 2e. Here, the gap of the DMN array is set to 750 μm. Taking the thicknesses of the epidermis and dermis into account, the length (i.e. height) of every DMN is set to 293 μm. The diameter of the bottom of the DMN is set to 142 μm, while the diameter of the top of the DMN is set to 15 μm, as shown in Fig. 2f. The setting of the top diameter is based on the mechanical analysis results, which will be described detailedly in the next section.

To fabricate the TCM DMN patch shown in Figs. 2d and 1 g TCM extracts (from EFONG Pharmaceutical Co., LTD, Foshan, Guangdong, China) and 9 g hyaluronic acid (HA-TLM-20-40, from Bloomage Biotechnology Co., LTD, Beijing, China) are dissolved in deionized water to obtain a base solution, as shown in Fig. 3a ∼ Fig. 3c. Afterwards, the basic solution is evenly stirred and vacuumed for rapid defoaming. Then, a high-pressure atomizer is applied to spray the base solution into a polydimethylsiloxane (PDMS) mold. After drying for 30 min at room temperature, a viscous hydrocolloid patch is finally adhered to the DMN array, and the TCM DMN patch is obtained after it is separated from the mold, as depicted in Fig. 3d. In this work, the PDMS mold is made on a metal master mold. Hence, based on the mature processing technique, 1000 TCM DMN patch have been easily fabricated. For every patch shown in Fig. 2d, the total mass is measured to be 10 mg, and the masses of the TCM extracts and HA are 1 mg and 9 mg, respectively. Furthermore, the masses of the 7 herbal extracts are 0.196 mg, 0.123 mg, 0.087 mg, 0.291 mg, 0.104 mg, 0.143 mg and 0.056 mg, respectively.

The size of the microneedle is directly introduced in this section. However, its mechanical properties have not been analyzed yet. In fact, research on the mechanical properties of the microneedle is very important because only if it smoothly penetrates the skin can the

Table 1
Paste rates, yield rates and ratios of the extracts of Chinese herbs used for sleep aid.

Type	Paste rate (%)	Yield rate (%)	Ratio (%)
Extract of Suan Zao Ren	18.5	25	19.6
Extract of Yuan Zhi	32	41.6	12.3
Extract of He Huan Hua	21	25	8.7
Extract of Shou Wu Teng	12.75	17	29.1
Extract of Wu Wei Zi	39.4	62.5	10.4
Extract of Lian Zi	19.5	32	14.3
Extract of Huang Lian	17	22	5.6

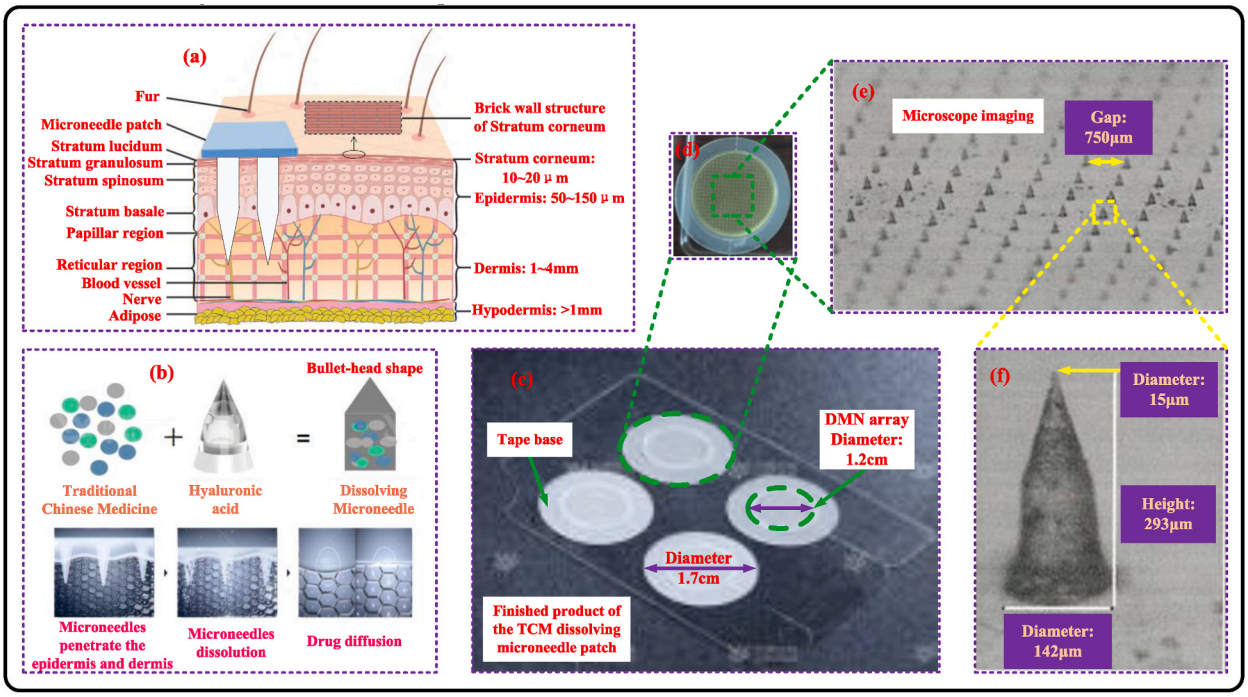

Fig. 2. a Schematic view of the cross section of human skin. **b** Design principle and action mechanism of the TCM dissolving microneedle patch. **c** Finished product of the TCM dissolving microneedle patch. **d** Physical picture of the TCM DMN patch; **e** Enlarged view of the microneedle array; **f** Enlarged view of one microneedle.

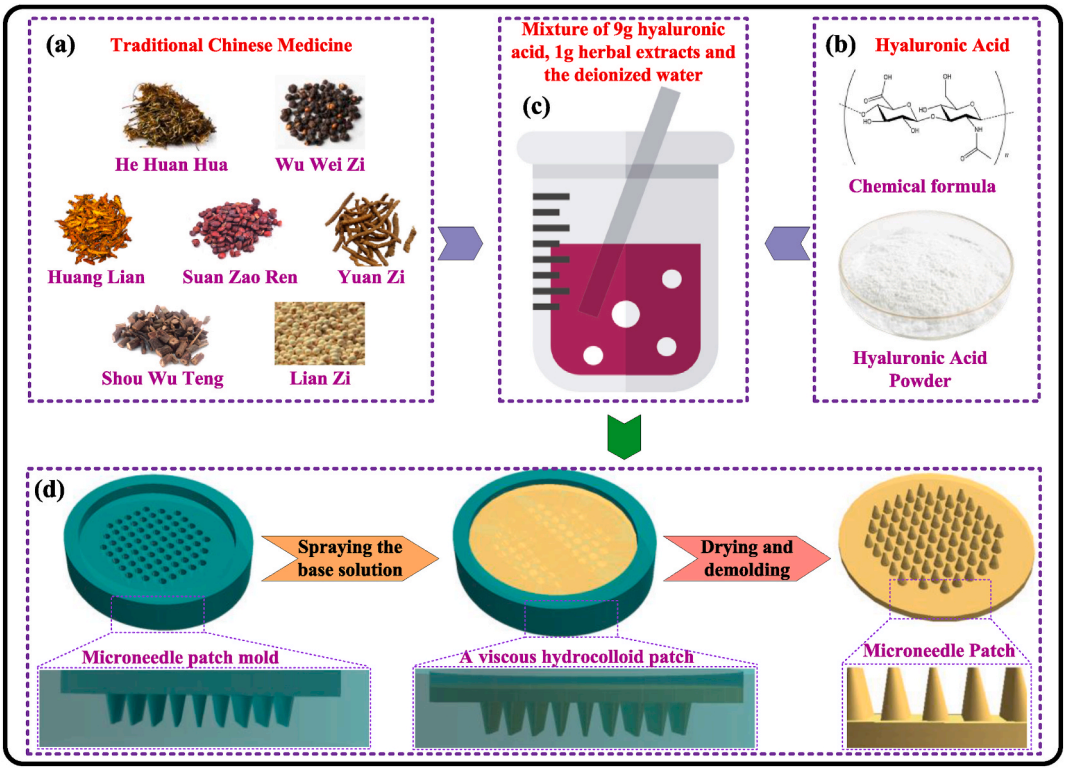

Fig. 3. a Seven Chinese herbs are used as the sleep-aid materials. **b** Hyaluronic acid is used as the carrier of the herbal extracts. **c** 9 g hyaluronic acid, 1 g TCM extracts and deionized water are mixed as a base solution. **d** Main fabrication flow of the TCM DMN patch.

drugs carried by the microneedle enter the body. Hence, the designed microneedle must have sufficient mechanical strength to penetrate the skin without breaking or bending. Due to the close correlation between the process of penetration into the skin and the skin structure, thus modelling and analyzing the skin mechanical properties can help to accurately evaluate the penetration ability of the designed microneedle. In addition, the shape of the microneedle is similar to a bullet head which consists of a cone and a cylinder. The diameter of the microneedle tip has a great influence on the mechanical properties, hence the piercing force and buckling force of the microneedles with different tip diameters should be analyzed and simulated.

2.3. Mechanical characteristic analysis method

In this section, the Finite Element Analysis (FEA) software Abaqus 6.14 is applied to model and simulate the behaviors of microneedles and epidermis during the penetration process.

2.3.1. Modelling of microneedle-skin interaction

All the MN tips used in the numerical modelling are conical. To get a better insight into the whole penetration process, the mechanical behavior of different skin layers should be studied first. The Young's modulus of the stratum corneum is over 24 times of that of the dermis [51]. Since the rests of the skin are much softer than the stratum corneum, MN is most likely to fail in the stratum corneum. Thus, only the effect of the stratum corneum should be considered. Therefore, the stratum corneum and the epidermis are regarded as the same layer, and its thickness is set to 120 μm for conservative estimation. The thickness of the hypodermis is set to 1 mm, as shown in Fig. 2a.

In this section, a nonlinear finite element analysis method based on the Abaqus/Explicit code is used to study the whole penetration process. To simplify the material model, the skin is regarded as an isotropic and incompressible hyper-elastic material, and the material properties related to the multi-layered human skin are shown in Table 2 [52,53]. The Neo-Hookean model is adopted as the skin constitutive model, which describes the constitutive relationship of hyper-elastic materials. The equation of the strain energy potential U is derived as (1) [54–56].

$$U = C_{10}(I_1 - 3) \tag{1}$$

where C_{10} is the material stiffness, and I_1 is the first invariant of the left Cauchy-Green deformation tensor.

Here, the microneedle is treated as a rigid body, whose shape and size do not change in any way under the action of external forces. The deformation of a rigid body requires a great force or pressure, and it cannot be restored to the original state after deformation. During the design process, it is necessary to analyze the load conditions to confirm whether the material meets the requirements of the structural strength and stiffness. Although there are many failure models, the models of maximum stress, maximum shear stress and Von Mises stress are the most commonly used. Strenkowski and Yan have demonstrated that the Von Mises stress failure criterion is the most suitable choice for simulating the failure and separation of hyper-elastic rubber materials. Hence, the Von Mises stress failure criterion is adopted in this work. Because the hyper-elastic models in Abaqus/Explicit do not incorporate the material failure mechanism, a special user material subroutine with a Von Mises stress failure criterion is put forward [57]. When the effective stress of the unit near the MN tip meets the failure criteria shown in (2), the unit will be identified and removed from the grid [46,58].

$$\sqrt{\left[(\sigma_1 - \sigma_2)^2 + (\sigma_2 - \sigma_3)^2 + (\sigma_3 - \sigma_1)^2\right] \Big/ 2} > \sigma \tag{2}$$

where, σ_1, σ_2, σ_3 represent the first, second and third principal stresses respectively, while σ represents the destructive strength of the stratum corneum. Therefore, according to the above principle, the piercing force of the MN with different tip diameters can be simulated.

2.3.2. Buckling analysis of the microneedle

The buckling force of the MN is relative to its length, yield strength and the tip's diameter. Big length, small yield strength and small tip's diameter may lead to the buckling failure [59]. Generally, the length is determined by the processing technique and industrial standard, and the yield strength is determined by the selected material. Thus, only the tip's diameter can be adjusted, and it is the emphasis of the buckling analysis. The critical load buckling force $F_{Buckling}$ can be calculated by the Euler's formula [48,60], as depicted in (3).

Table 2
Material parameters of the multi-layered human skin model.

Parameter	Stratum corneum	Dermis	Hypodermis
Density (kg/m^3)	1300	1230	1230
Failure stress (MPa)	28.5	8.4	7.3
Young's modulus (MPa)	120	5	0.5
Poisson's ratio	0.39	0.48	0.48

$$F_{Buckling} = \frac{\pi EI}{(KL)^2} \tag{3}$$

Where, E is the elasticity modulus, I is the area moment of inertia, L is the length and K is the effective length factor. The buckling analysis of the MN is performed using Abaqus 6.14 software. The conical MN is created with a height of 293 μm, base diameter of 142 μm. The created model is fine-meshed using a quadratic 3D stress element (C3D10). To predict the buckling shape and critical buckling load, the linear analysis method is adopted here. During the linear buckling analysis, a compression load of 1 N is applied on the top surface of the MN. The simulation flow is set up with a buckle-linear perturbation procedure.

2.4. Evaluation method for sleep-aid effect

The test results of EEG, functional Near-Infrared Spectroscopy (fNIRS), and functional Magnetic Resonance Imaging (fMRI) indicate that the frontal lobe plays a crucial role in maintaining sleep [61–63]. In the Non-Rapid Eye Movement (NREM) stage, the prefrontal cortex and thalamus are less inactivated in insomnia patients, and the metabolism of the frontoparietal cortex is relatively large [64]. What's more, Joy Perrier et al. studied the prefrontal neural activities in the patients with primary insomnia, who exhibited a higher beta wave energy and a lower delta wave energy [65]. In our previous work, the single-lead EEG signal of the prefrontal lobe has been proved to be effective for the sleep-aid effect evaluation [66], so it is also adopted in this work. The experimental platform is set up, as illustrated in Fig. 4a, and the Bioelectrical Signal Acquisition (BSA) circuit is utilized to acquire the tiny EEG signal. The effective frequency range of the EEG signal is 0.3–64 Hz, with an amplitude range of 10–200 μV. Therefore, the main function of the BSA circuit is to amplify the weak signal and filter the noise.

The BSA circuit is composed of a Low Pass Filter (LPF), an instrumentation amplifier combined a High Pass Filter (HPF), a HPF, a LPF combined an adder. The total gain of the BSA circuit is set to about 4000. The cut-off frequencies of the two first-order LPFs are both set to 0.3 Hz, while the cut-off frequencies of the two first-order HPFs are both set to 63.7 Hz. The adder is applied to make the output signal be between 0 and V_{dd}, because the input of the Analog to Digital Converter (ADC) of a Microprogrammed Control Unit (MCU) should be larger than 0. V_{dd} and V_{ss} are the positive and negative power supply, respectively. Here, AD8421 and AD8676 (made

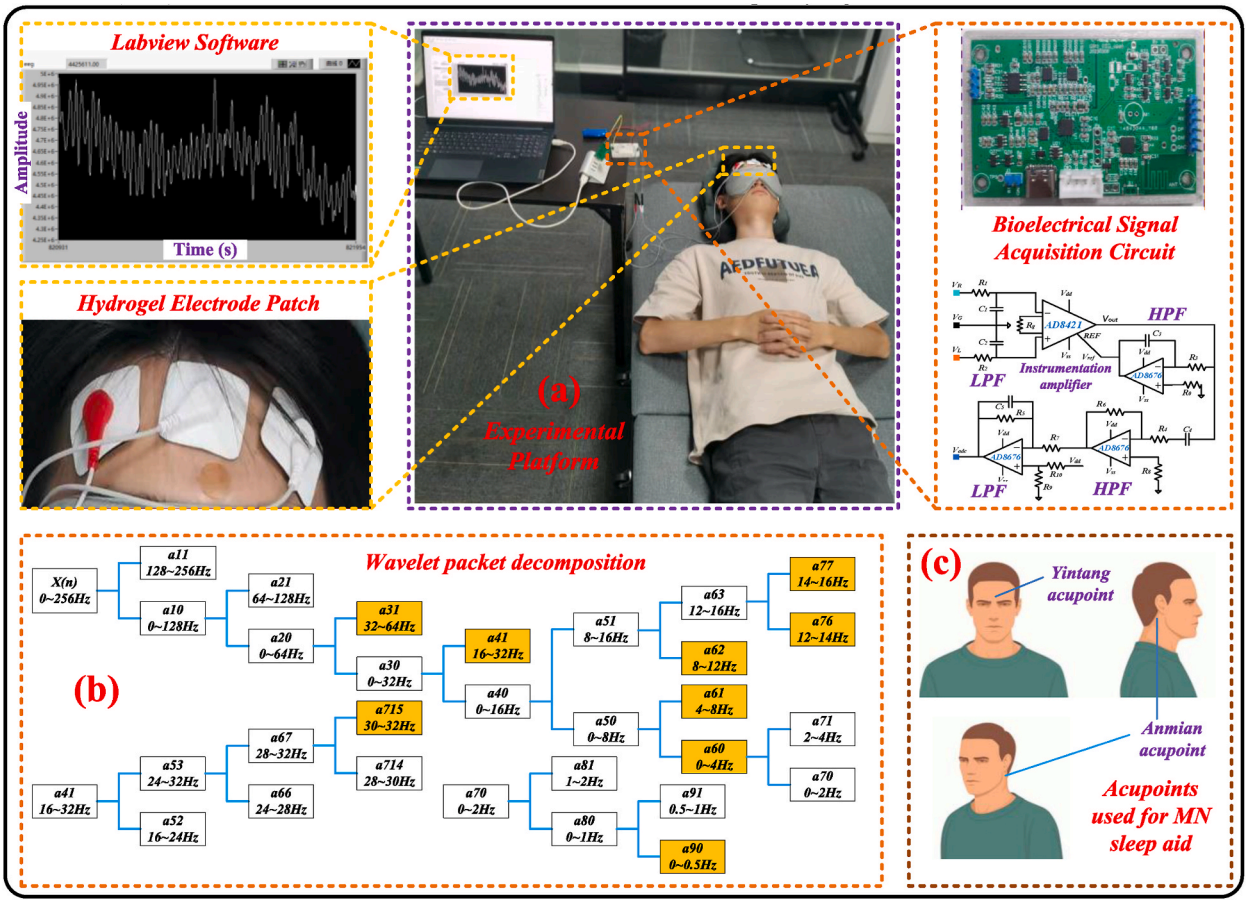

Fig. 4. a Experimental platform is set up for evaluating the sleep-aid effect of the MN patch. **b** Decomposition tree of 9-level tower wavelet packet transform. **c** Anmian and Yintang acupoints are used for MN sleep aid.

by USA Analog Devices Co. Ltd.) are chosen as the instrumentation amplifier and operational amplifier, respectively. CS32A010 (made by Chipsea Co., Ltd. Shenzhen, China) is selected as the edge-computing MCU. The sampling frequency f_s of the ADC is set as 512 Hz, because the effective EEG signal is a low-frequency signal.

On the other hand, in order to reduce the contact impedance of the skin, the hydrogel electrodes are used for EEG signal acquisition. A lithium battery is applied to power the BSA circuit to avoid the power-line interference. LabVIEW software is utilized to collect the sampling data and make them visual at real time. After data acquisition, Wavelet Packet Decomposition (WPD) is used to extract different brainwave signals, as shown in Fig. 4b. According to the frequency band, EEG signal can be divided into five categories, namely delta wave (0.5–4 Hz), theta wave (4–8 Hz), alpha wave (8–14 Hz), beta wave (14–30 Hz) and gamma wave (30–64 Hz). Therefore, these five signals can be extracted by (4). Where, *wpdec* is a one-dimensional (1D) wavelet packet decomposition function, and wavelet function is chosen as '*db6*'. *wpt* is a wavelet packet tree object corresponding to the WPD of the input signal $\boldsymbol{X_{EEG}}$ at level 9. *wprcoef* is a 1D or two-dimensional (2D) WPD function, and [62] means node 2 at level 6. Thus the reconstructed signal of the node 0 at level 9, namely baseline, stands for the low-frequency signal in the frequency band of 0∼0.5 Hz. It is a low-frequency bias drift, which should be eliminated.

$$\begin{cases} wpt = wpdec(X_{EEG}, 9, 'db6') \\ baseline = wprcoef(wpt, [9\ 0]) \\ S_{delta} = wprcoef(wpt, [6\ 0]) - baseline \\ S_{theta} = wprcoef(wpt, [6\ 1]) \\ S_{alpha} = wprcoef(wpt, [6\ 2]) + wprcoef(wpt, [7\ 6]) \\ S_{beta} = wprcoef(wpt, [4\ 1]) + wprcoef(wpt, [7\ 7]) \\ -wprcoef(wpt, [7\ 15]) \\ S_{gamma} = wprcoef(wpt, [3\ 1]) + wprcoef(wpt, [7\ 15]) \end{cases} \tag{4}$$

S_{delta}, S_{theta}, S_{alpha}, S_{beta} and S_{gamma} are the signals of delta, theta, alpha, beta and gamma waves, respectively. Thus their energy integrals, E_{delta}, E_{theta}, E_{alpha}, E_{beta} and E_{gamma}, can be calculated as (5).

$$\begin{cases} E_{delta} = \int_{0.5}^{4} AM_{delta}^2(f)df \\ E_{theta} = \int_{4}^{8} AM_{theta}^2(f)df \\ E_{alpha} = \int_{8}^{14} AM_{alpha}^2(f)df \\ E_{beta} = \int_{14}^{30} AM_{beta}^2(f)df \\ E_{gamma} = \int_{30}^{64} AM_{gamma}^2(f)df \end{cases} \tag{5}$$

Where, $AM_{delta}(f)$, $AM_{theta}(f)$, $AM_{alpha}(f)$, $AM_{beta}(f)$ and $AM_{gamma}(f)$ are the amplitude functions of delta, theta, alpha, beta and gamma waves respectively after Fast Fourier Transform (FFT) analysis. The delta, theta and alpha waves are slow wave signals, and the higher their energies, the better they indicate relaxation and good sleep. The beta and gamma waves are fast wave signals, and the higher their energies, the more nervous and alert they are. Here, an energy ratio R_{LH} is introduced and defined as (6).

$$R_{LH} = \frac{E_{delta} + E_{theta} + E_{alpha}}{E_{beta} + E_{gamma}} \tag{6}$$

Hence, based on the analysis above, if the sleep-aid method is effective, R_{LH} will increase compared with the initial value R_{LH0} before sleep-aid intervention. Thus, R_{LH} can be applied to evaluate the sleep-aid effect.

2.5. Experimental scheme

According to the principle of TCM, the basic pathogenesis of insomnia is restlessness and imbalance of Yin and Yang. Hence, the treatment should focus on the Du Vessel, Hand Shaoyin and Foot Taiyin meridians. Given that the acupoints on the forehead are more conducive to assisting sleep, and it is best to have no hair blocking the acupoints, thus the acupoints of Yintang and Anmian are finally selected for sleep aid, as depicted in Fig. 4c. For evaluating the sleep-aid effect of the proposed MN patch, in this work, 8 subjects with mild insomnia were recruited to take part in the experimental tests. All recruited participants received the oral and written descriptions of the experiment before the tests, signed informed consent forms, and obtained approval from the institutional review committee (reference number: GDUTXS2024017). The inclusion criterion included the healthy adults aged over 18. Exclusion criterion included someone suffered from serious illnesses or had difficulty in finishing the long test. For each subject, one patch was affixed to the Yintang acupoint and two were affixed to the Anmian acupoints before going to bed every day. These sleep-aid MN patches generally dissolved and absorbed within 1 h. The sleep-aid experiment lasted for 3 weeks. For comparison, during the sleep-aid process of MN patches, the EEG signals within 30 min of the first day and the last day were acquired. Afterwards, R_{LH0} before the sleep-aid intervention and R_{LH} after the sleep-aid intervention were calculated and compared.

3. Results and discussion

3.1. Mechanical characteristic analysis results

Firstly, numerical simulation of microneedle-skin interaction was conducted with Abaqus 6.14. There are 4 stages during the penetration process, as shown in Fig. 5a. Assuming that t represents the simulation time, then the performances of the MN in 4 stages are as follows:

Stage 1. When $t = 0.0011$ s, the MN tip is ready to contact the skin surface, and the skin has not deformed.

Stage 2. When $t = 0.0031$ s, the MN tip is in contact with the skin surface, resulting in the increases of the curvature and deformation of the skin. The maximum Mises stress reaches 22.65 MPa.

Stage 3. When t = 0.0034 s, the maximum Mises stress reaches 25.26 MPa, which is close to the damage limit stress of the stratum corneum, namely 28.5 MPa. The bending deformation of the skin continues to increase. Compared with that in stage 2, and the stratum corneum is about to be penetrated.

Stage 4. When t = 0.0035 s, the maximum Mises stress decreases to 24.08 MPa. Since the MN tip has completely penetrated the stratum corneum, the maximum Mises stress decreases gradually.

In addition, it is very important to study the piercing force and buckling force. For different MN tips, they are different. Here, the tips with three different radii, namely 5 μm, 15 μm and 22 μm, are selected for simulation analysis, as depicted in Fig. 5b. After Abaqus simulation, the relationship between force and penetration depth is illustrated in Fig. 5c. It demonstrates that the piercing force of the three tips are 0.014 N, 0.033 N and 0.075 N, respectively. The smaller the radius of the MN tip, the smaller the piercing force. The piercing force and buckling force of the three tips are depicted in Fig. 5d. It is clear that the piercing force is larger than the buckling

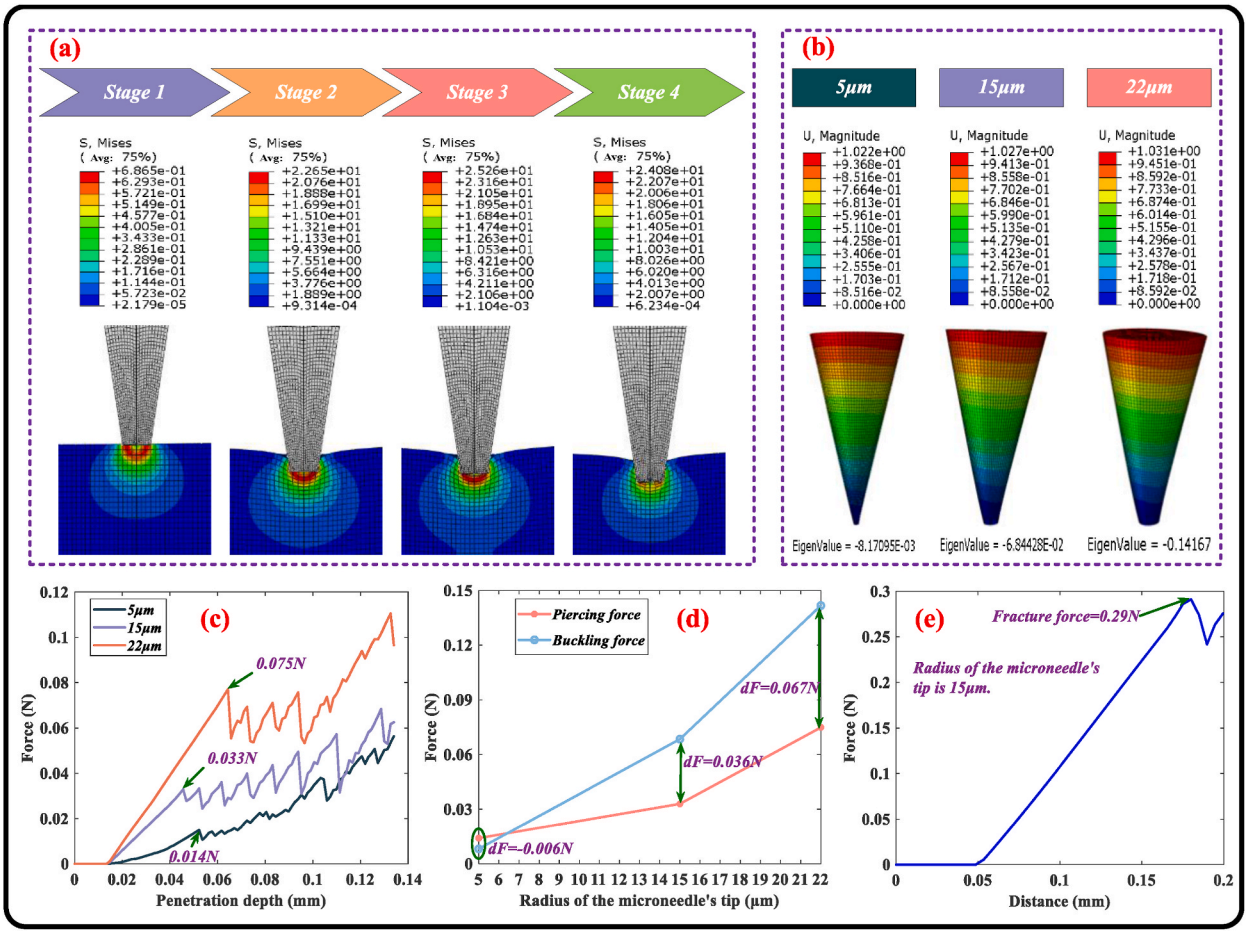

Fig. 5. a There are 4 stages during the MN penetration process. **b** The tips with three different radii, namely 5 μm, 15 μm and 22 μm, are selected for simulation analysis. **c** The exciting force varies with the penetration depth. **d** The piercing force and buckling force vary with the radius of the MN tip. **e** The measured exciting force varies with the moving distance when the tip radius is set to 15 μm.

force when the radius of the MN tip is 5 μm, resulting in the unsuccessful penetration into the skin. However, this issue can be solved and the piercing force is smaller than the buckling force when the radius of the MN tip is enlarged to 15 μm or 22 μm. At this case, the difference between the piercing force and buckling force is 0.036 N or 0.067 N, resulting in the successful penetration into the skin. In this work, the design principle is that the MN can easily penetrate the skin without bending or breaking. That is, the piercing force should be small, and the margin between the piercing force and buckling force should be large. Therefore, after comprehensive consideration, the radius of the MN tip is finally set to 15 μm, instead of 22 μm.

To further confirm the penetration ability of the MN, the vertical breaking force test for a single microneedle was conducted, and the measured result is shown in Fig. 5e. It figures out that the fracture force of the MN with radius of 15 μm is about 0.29 N, which is about 5 times of the buckling force, and 10 times of the piercing force. Hence, the MN patch can penetrate the skin smoothly.

3.2. Sleep-aid test results

8 subjects were recruited to take part in the sleep-aid tests, and the experiment lasted for 3 weeks. The EEG signal tests were performed at the first day and the last day. The raw EEG signals are shown in Fig. 6a. In order to extract the delta, theta, alpha, beta and gamma waves, wavelet packet decomposition and reconstruction were conducted, as shown in Fig. 6b. Then, FFT analysis was applied to obtain the frequency response, as illustrated in Fig. 6c. It indicates that this signal separation method is effective since the spectrums of the five waves accord with the definitions mentioned above.

Thus, the energy integrals E_{delta}, E_{theta}, E_{alpha}, E_{beta} and E_{gamma} can be obtained after FFT analysis. With Equation (6), R_{LH0} and R_{LH} can be calculated, as listed in Table 3. It demonstrates that for 6 subjects (P1, P3, P4, P6, P7 and P8) the energy ratios R_{LH} are larger than the energy ratios R_{LH0}, while the results of the rest 2 subjects (P2 and P5) are opposite. After sleep-aid intervention on the Anmian and Yintang acupoints using the MN patches, for most subjects, there are obvious increases of the ratios of the low-frequency brain wave energies to the high-frequency brain wave energies, indicating that the proposed sleep-aid method is effective. On the other hand, the data are applied for the statistics analysis with *t*-test, and the *P*-value is larger than 0.05, indicating that there is no significant difference. It may be related to the insufficient sample size, and the *P*-value may be decreased by increasing the number of the subjects.

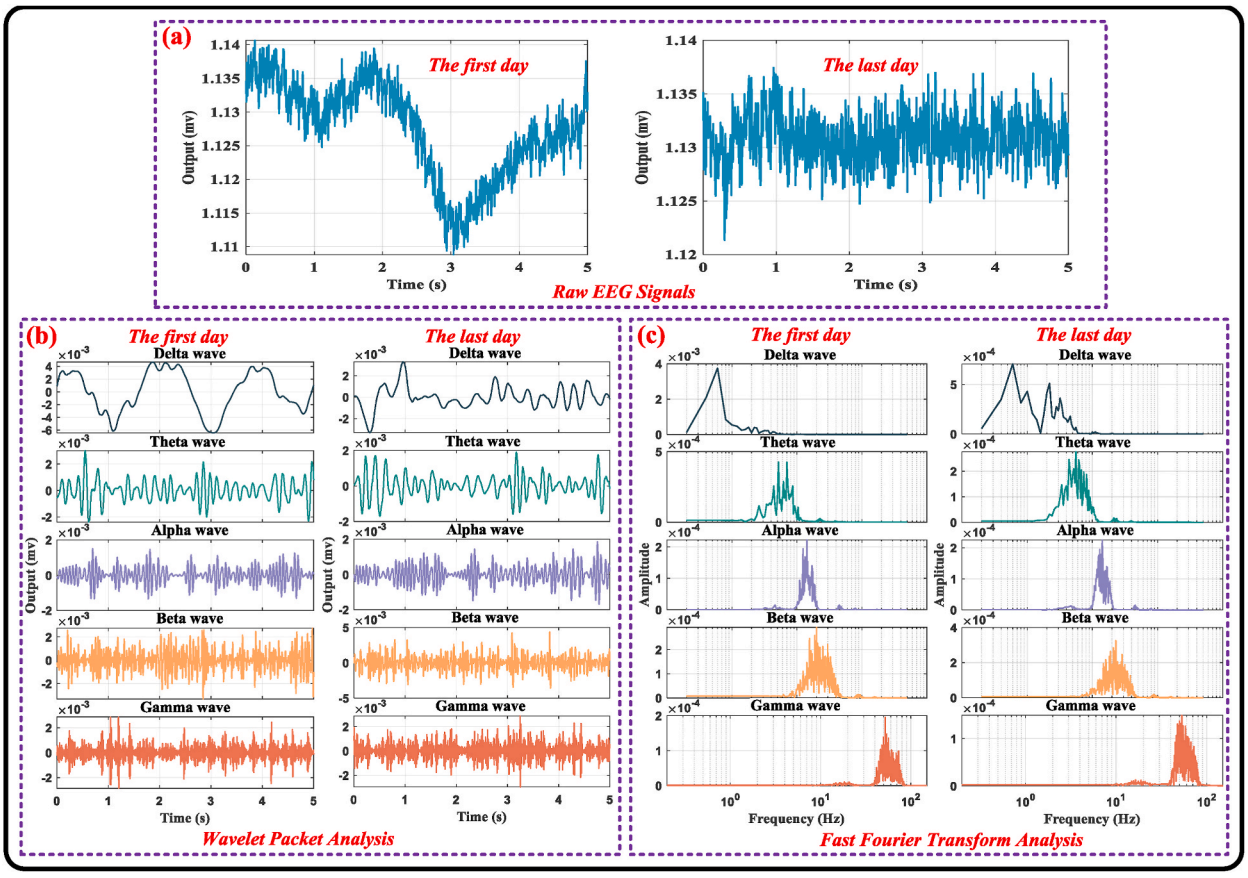

Fig. 6. a EEG signals were measured at the first day and the last day. **b** Delta, theta, alpha, beta, gamma waves were extracted by wavelet package decomposition and reconstruction. **c** FFT analysis was conducted for delta, theta, alpha, beta, gamma waves.

Table 3
Energy ratios of the subjects were measured at the first day and the last day.

Subject	R_{LH0}	R_{LH}
P1	30.50	40.89
P2	15.04	0.90
P3	4.06	26.20
P4	42.74	57.66
P5	52.79	4.91
P6	15.86	21.95
P7	19.29	20.81
P8	4.56	41.49

3.3. Limitation

The number of the subjects in this work is very small. They are mainly young people, mild or ultra mild insomniacs, which leads to the less significant results. In the future, more subjects of different ages and levels of insomnia will be recruited for the experimental tests. In addition, the foreign body sensation caused by the MN patch makes some subjects uncomfortable, which may be the reason for the opposite results of the subjects P2 and P5. Therefore, it is necessary to continuously optimize the materials of the MN patch and improve the user experience. These will be our future work.

4. Conclusions

In this paper, a flexible and dissolving TCM microneedle patch is proposed for sleep-aid intervention. The materials, design method and fabrication process of the microneedle patch have been described in detail. Besides, mechanical characteristics of the microneedle patch and sleep-aid effect evaluation method have been also presented. Abaqus simulation results indicate that the smaller the radius of the microneedle tip, the smaller the piercing force. Considering that the microneedle should easily penetrate the skin without buckling, that is, the piercing force should be larger than the buckling force, thus 15 μm, instead of 5 μm or 22 μm, is more suitable to be adopted as the radius of the microneedle tip. For the microneedle with the radius of 15 μm, the piercing force is 0.033 N, and the difference between the piercing force and buckling force is 0.036 N. Experimental results demonstrate that the fracture force of the microneedle is about 0.29 N, which is far larger than the piercing force and buckling force. Hence, the simulation results accord with the experimental results. After sleep-aid intervention on the Anmian and Yintang acupoints using the patches, for most subjects, the ratios of the low-frequency brain wave energies to the high-frequency brain wave energies are increased obviously, indicating that the proposed sleep-aid method is effective.

To sum up, this microneedle patches can be used for sleep-aid intervention at home, which is low-cost, convenient and comfortable. Given that the sleep-aid effect may vary from person to person, the proposed sleep-aid method should be further verified and improved by more subjects. The improvement aiming to the above limitation will be our future work.

Data availability statement

The authors do not have permission to share data.

Ethics declarations

This study was reviewed and approved by the ethics committee of Guangdong University of Technology, with the approval number: GDUTXS2024017.

CRediT authorship contribution statement

Chunhua He: Writing – original draft, Funding acquisition, Conceptualization. **Zewen Fang:** Writing – original draft, Software, Investigation. **Heng Wu:** Validation, Methodology. **Xiaoping Li:** Writing – review & editing, Data curation. **Lianglun Cheng:** Project administration. **Yangxing Wen:** Visualization, Resources. **Juze Lin:** Writing – review & editing, Formal analysis.

Declaration of competing interest

The authors declare that they have no known competing financial interests or personal relationships that could have appeared to influence the work reported in this paper.

Acknowledgements

This work was supported by the National Natural Science Foundation of China (Grant Nos. 62104047, U22A2012 and 62173098), Guangdong Basic and Applied Basic Research Foundation (Grant No. 2023A1515010291), and Basic and Applied Basic Research

Foundation of Guangzhou Basic Research Program (Grant No. 2023A04J1707).

Abbreviations

Chinese Herbal Medicine CHM
Traditional Chinese Medicine TCM
Benzodiazepine receptor agonists BZRAs
Non-benzodiazepine hypnotics non-BZDs
Cognitive Behavioral Therapy for Insomnia CBTI
Non-invasive Brain Stimulation NIBS
Transcranial Current Stimulation TCS
Transcranial Magnetic Stimulation TMS
Microneedle MN
Stratum Corneum SC
Dissolving MN DMN
Hyaluronic Acid HA
Sprague Dawley SD
ElectroEncephaloGraphy EEG
Cosmetic Ingredients Catalog CIC
International Nomenclature Cosmetic Ingredient INCI
International Cosmetic Ingredient Dictionary and Handbook ICIDH
Material Safety Data Sheet MSDS
Certificate of Analysis COA
Polydimethylsiloxane PDMS
Finite Element Analysis FEA
functional Near-Infrared Spectroscopy fNIRS
functional Magnetic Resonance Imaging fMRI
Non-Rapid Eye Movement NREM
Bioelectrical Signal Acquisition BSA
Low Pass Filter LPF
High Pass Filter HPF
Analog to Digital Converter ADC
Microprogrammed Control Unit MCU
Wavelet Packet Decomposition WPD
Fast Fourier Transform FFT

References

[1] M.L. Perlis, D. Posner, D. Riemann, C.H. Bastien, J. Teel, M. Thase, Insomnia, Lancet 400 (2022) 1047–1060, https://doi.org/10.1016/s0140-6736(22)00879-0.
[2] C.E. Carney, J.D. Edinger, M. Kuchibhatla, A.M. Lachowski, O. Bogouslavsky, A.D. Krystal, C.M. Shapiro, Cognitive behavioral insomnia therapy for those with insomnia and depression: a randomized controlled clinical trial, Sleep 40 (2017) zsx019, https://doi.org/10.1093/sleep/zsx019.
[3] M.S. Pluzhnikov, A.A. Blotskii, [Epidemiology and laser correction of chronic diseases observed in snoring and obstructive sleep apnea], Vestn. Otorinolaringol. 3 (2002) 12–15.
[4] M.A. Rainer, P.H. Palmer, B. Xie, Sleep duration and chronic disease Among older native hawaiians or other pacific islanders and asians: analysis of the behavioral risk factor surveillance system, Journal of Racial and Ethnic Health Disparities 10 (2023) 2302–2311, https://doi.org/10.1007/s40615-022-01409-0.
[5] Y. You, X. Zhong, G. Liu, Z. Yang, Automatic sleep stage classification: a light and efficient deep neural network model based on time, frequency and fractional Fourier transform domain features, Artif. Intell. Med. 127 (2022) 102279, https://doi.org/10.1016/j.artmed.2022.102279.
[6] E. Jeong, K.S. Cha, H.-R. Shin, E.Y. Kim, J.-S. Jun, T.-J. Kim, J.-I. Byun, J.-W. Shin, J.-S. Sunwoo, K.-Y. Jung, Alerting network alteration in isolated rapid eye movement sleep behavior disorder patients with mild cognitive impairment, Sleep Med. 89 (2022) 10–18, https://doi.org/10.1016/j.sleep.2021.11.002.
[7] E. Matheson, B.L. Hainer, Insomnia: Pharmacologic Therapy, 96, American family physician, 2017, pp. 29–35.
[8] T. Roehrs, J. Verkler, G. Koshorek, T. Roth,Sleep Disorders in Addiction: An Overview, Textbook of Addiction Treatment: Int. Perspect., https://doi.org/10.1007/978-3-030-36391-8_83.
[9] T. Roth, D. Seiden, S. Wang-Weigand, J. Zhang, A 2-night, 3-period, crossover study of ramelteon's efficacy and safety in older adults with chronic insomnia, Curr. Med. Res. Opin. 23 (2007) 1005–1014, https://doi.org/10.1185/030079907X178874.
[10] A.D. Krystal, A. Lankford, H.H. Durrence, E. Ludington, P. Jochelson, R. Rogowski, T. Roth, Efficacy and safety of doxepin 3 and 6 mg in a 35-day sleep laboratory trial in adults with chronic primary insomnia, Sleep 34 (2011) 1433–1442, https://doi.org/10.5665/SLEEP.1294.
[11] F. Li, B. Xu, H. Shi, T. Zhang, Z. Song, Y. Chen, L. Liu, P. Wang, Efficacy and safety of TCM Yangxin Anshen Therapy for insomnia: a systematic review and meta-analysis, Medicine 99 (2020) e19330.
[12] A. Van Straten, T. van der Zweerde, A. Kleiboer, P. Cuijpers, C.M. Morin, J. Lancee, Cognitive and behavioral therapies in the treatment of insomnia: a meta-analysis, Sleep Med. Rev. 38 (2018) 3–16, https://doi.org/10.1016/j.smrv.2017.02.001.
[13] M.R. Ebben, P. Yan, A.C. Krieger, The effects of white noise on sleep and duration in individuals living in a high noise environment in New York City, Sleep Med. 83 (2021) 256–259, https://doi.org/10.1016/j.sleep.2021.03.031.
[14] E. Lattari, S.S. Costa, C. Campos, A.J. de Oliveira, S. Machado, G.A.M. Neto, Can transcranial direct current stimulation on the dorsolateral prefrontal cortex improves balance and functional mobility in Parkinson's disease? Neurosci. Lett. 636 (2017) 165–169, https://doi.org/10.1016/j.neulet.2016.11.019.

[15] N. Sun, Y. He, Z. Wang, W. Zou, X. Liu, The effect of repetitive transcranial magnetic stimulation for insomnia: a systematic review and meta-analysis, Sleep Med. 77 (2021) 226–237, https://doi.org/10.1016/j.sleep.2020.05.020.
[16] L. Krone, L. Frase, H. Piosczyk, P. Selhausen, S. Zittel, F. Jahn, M. Kuhn, B. Feige, F. Mainberger, S. Klöppel, Top-down control of arousal and sleep: fundamentals and clinical implications, Sleep Med. Rev. 31 (2017) 17–24, https://doi.org/10.1016/j.smrv.2015.12.005.
[17] X. Yin, M. Gou, J. Xu, B. Dong, P. Yin, F. Masquelin, J. Wu, L. Lao, S. Xu, Efficacy and safety of acupuncture treatment on primary insomnia: a randomized controlled trial, Sleep Med. 37 (2017) 193–200, https://doi.org/10.1016/j.sleep.2017.02.012.
[18] Y. Lu, Y. Huang, C. Tang, B. Shan, S. Cui, J. Yang, J. Chen, R. Lin, H. Xiao, S. Qu, Brain areas involved in the acupuncture treatment of AD model rats: a PET study, BMC Compl. Alternative Med. 14 (2014) 1–8, https://doi.org/10.1186/1472-6882-14-178.
[19] J. Xiong, Z. Zhang, Y. Ma, Z. Li, F. Zhou, N. Qiao, Q. Liu, W. Liao, The effect of combined scalp acupuncture and cognitive training in patients with stroke on cognitive and motor functions, NeuroRehabilitation 46 (2020) 75–82, https://doi.org/10.3233/NRE-192942.
[20] X. Yin, M. Gou, J. Xu, B. Dong, P. Yin, F. Masquelin, J. Wu, L. Lao, S. Xu, Efficacy and safety of acupuncture treatment on primary insomnia: a randomized controlled trial, Sleep Med. 37 (2017) 193–200, https://doi.org/10.1016/j.sleep.2017.02.012.
[21] J.L. Shergis, X. Ni, M.L. Jackson, A.L. Zhang, X. Guo, Y. Li, C. Lu, C.C. Xue, A systematic review of acupuncture for sleep quality in people with insomnia, Compl. Ther. Med. 26 (2016) 11–20, https://doi.org/10.1016/j.ctim.2016.02.007.
[22] C. Fu, N. Zhao, Z. Liu, L.-h. Yuan, C. Xie, W.-j. Yang, X.-t. Yu, H. Yu, Y.-f. Chen, Acupuncture improves peri-menopausal insomnia: a randomized controlled trial, Sleep 40 (2017) zsx153, https://doi.org/10.1093/sleep/zsx153.
[23] L.L. Zhong, N. Shi, Y. Sun, B.F. Ng, Z. Bian, A. Lu, Hong Kong Chinese medicine clinical practice guideline for insomnia, European Journal of Integrative Medicine 39 (2020) 101193, https://doi.org/10.1016/j.eujim.2020.101193.
[24] S.M. Pyo, H.I. Maibach, Skin metabolism: relevance of skin enzymes for rational drug design, Skin Pharmacol. Physiol. 32 (2019) 283–294, https://doi.org/10.1159/000501732.
[25] Z. Sartawi, C. Blackshields, W. Faisal, Dissolving microneedles: applications and growing therapeutic potential, J. Contr. Release 348 (2022) 186–205, https://doi.org/10.1016/j.jconrel.2022.05.045.
[26] L. Zhang, R. Guo, S. Wang, X. Yang, G. Ling, P. Zhang, Fabrication, evaluation and applications of dissolving microneedles, Int. J. Pharm. 604 (2021) 120749, https://doi.org/10.1016/j.ijpharm.2021.120749.
[27] J. Yang, X. Wang, D. Wu, K. Yi, Y. Zhao, Yunnan Baiyao-loaded multifunctional microneedle patches for rapid hemostasis and cutaneous wound healing, J. Nanobiotechnol. 21 (2023) 178.
[28] M.T. McCrudden, E. McAlister, A.J. Courtenay, P. González-Vázquez, T.R. Raj Singh, R.F. Donnelly, Microneedle applications in improving skin appearance, Exp. Dermatol. 24 (2015) 561–566, https://doi.org/10.1111/exd.12723.
[29] Z. Qi, J. Cao, X. Tao, X. Wu, S.C. Kundu, S. Lu, Silk fibroin microneedle patches for the treatment of insomnia, Pharmaceutics 13 (2021) 2198, https://doi.org/10.3390/pharmaceutics13122198.
[30] L. Zhu, S. Zhang, X. Yu, S. Zhu, G. Ou, Q. Li, Y. Zhang, L. Wang, X. Zhuang, L. Du, Application of armodafinil-loaded microneedle patches against the negative influence induced by sleep deprivation, Eur. J. Pharm. Biopharm. 169 (18) (2021) 178, https://doi.org/10.1016/j.ejpb.2021.10.009.
[31] K. Choi, Y.J. Lee, S. Park, N.K. Je, H.S. Suh, Efficacy of melatonin for chronic insomnia: systematic reviews and meta-analyses, Sleep Med. Rev. 66 (2022) 101692, https://doi.org/10.1016/j.smrv.2022.101692.
[32] J.M. Jerry, N. Shirvani, R. Dale, Addiction to armodafinil and modafinil presenting with paranoia, J. Clin. Psychopharmacol. 36 (2016) 98–100, https://doi.org/10.1097/jcp.0000000000000446.
[33] J. Chi, L. Sun, L. Cai, L. Fan, C. Shao, L. Shang, Y. Zhao, Chinese herb microneedle patch for wound healing, Bioact. Mater. 6 (2021) 3507–3514, https://doi.org/10.1016/j.bioactmat.2021.03.023.
[34] X. Ning, C. Wiraja, W.T.S. Chew, C. Fan, C. Xu, Transdermal delivery of Chinese herbal medicine extract using dissolvable microneedles for hypertrophic scar treatment, Acta Pharm. Sin. B 11 (2021) 2937–2944.
[35] S.N. Haynes, A. Adams, M. Franzen, The effects of presleep stress on sleep-onset insomnia, J. Abnorm. Psychol. 90 (1981) 601, https://doi.org/10.1037//0021-843x.90.6.601.
[36] S.N. Haynes, D.R. Follingstad, W.T. McGowan, Insomnia: sleep patterns and anxiety level, J. Psychosom. Res. 18 (1974) 69–74, https://doi.org/10.1016/0022-3999(74)90069-5.
[37] R.R. Freedman, H.L. Sattler, Physiological and psychological factors in sleep-onset insomnia, J. Abnorm. Psychol. 91 (1982) 380, https://doi.org/10.1037//0021-843x.91.5.380.
[38] R.R. Freedman, EEG power spectra in sleep-onset insomnia, Electroencephalogr. Clin. Neurophysiol. 63 (1986) 408–413, https://doi.org/10.1016/0013-4694(86)90122-7.
[39] B.A. Riedner, M.R. Goldstein, D.T. Plante, M.E. Rumble, F. Ferrarelli, G. Tononi, R.M. Benca, Regional patterns of elevated alpha and high-frequency electroencephalographic activity during nonrapid eye movement sleep in chronic insomnia: a pilot study, Sleep 39 (2016) 801–812, https://doi.org/10.5665/sleep.5632.
[40] M. Seeck, L. Koessler, T. Bast, F. Leijten, C. Michel, C. Baumgartner, B. He, S. Beniczky, The standardized EEG electrode array of the IFCN, Clin. Neurophysiol. 128 (2017) 2070–2077, https://doi.org/10.1016/j.clinph.2017.06.254.
[41] B.P. Lucey, J.S. Mcleland, C.D. Toedebusch, J. Boyd, J.C. Morris, E.C. Landsness, K. Yamada, D.M. Holtzman, Comparison of a single-channel EEG sleep study to polysomnography, J. Sleep Res. 25 (2016) 625–635, https://doi.org/10.1111/jsr.12417.
[42] B.L. Radhakrishnan, E. Kirubakaran, I.J. Jebadurai, K. Gurudev, Classifying Sleep Stages Automatically in Single-Channel against Multi-Channel EEG: A Performance Analysis, Springer Nature Singapore, Singapore, 2022, pp. 527–537.
[43] P.-L. Lee, Y.-H. Huang, P.-C. Lin, Y.-A. Chiao, J.-W. Hou, H.-W. Liu, Y.-L. Huang, Y.-T. Liu, T.-D. Chiueh, Automatic sleep staging in patients with obstructive sleep apnea using single-channel frontal EEG, J. Clin. Sleep Med. 15 (2019) 1411–1420, https://doi.org/10.5664/jcsm.7964.
[44] M. Yang, H. Wang, Y.L. Zhang, F. Zhang, X. Li, S.-D. Kim, Y. Chen, J. Chen, S. Chimonas, D. Korenstein, The Herbal Medicine Suanzaoren (Ziziphi Spinosae Semen) for sleep quality improvements: a systematic review and meta-analysis, Integr. Cancer Ther. 22 (2023), https://doi.org/10.1177/15347354231162080.
[45] K.-X. Hao, C.-Y. Shen, J.-G. Jiang, Sedative and hypnotic effects of Polygala tenuifolia willd. saponins on insomnia mice and their targets, J. Ethnopharmacol. 323 (2024) 117618, https://doi.org/10.1016/j.jep.2023.117618.
[46] P. Lu, C. Zhang, J. Zheng, C. Li, Q. Zhang, B. Huang, A comparison review of Hehuan flowers and Hehuan bark on the traditional applications, phytochemistry and pharmacological effects, J. Ethnopharmacol. 303 (2023) 116002, https://doi.org/10.1016/j.jep.2022.116002.
[47] C.-h. Ko, C.-m. Koon, S.-l. Yu, K.-y. Lee, C.B.-s. Lau, E.H.-y. Chan, Y.-k. Wing, K.-p. Fung, P.-c. Leung, Hypnotic effects of a novel anti-insomnia formula on Drosophila insomnia model, Chin. J. Integr. Med. 22 (2016) 335–343, https://doi.org/10.1007/s11655-014-1625-1.
[48] K. Liang, T. Qiao, N. Sun, N. Jiang, F. Li, H. Jiang, Y. Jiang, Mechanism of schisandra chinensis in treatment of insomnia by sleep–wake cycle based on network pharmacology, Phcog. Mag. (2023), https://doi.org/10.1177/09731296231216171.
[49] M. Wang, W.-J. Hu, Q.-h. Wang, B.-y. Yang, H.-x. Kuang, Extraction, purification, structural characteristics, biological activities, and application of the polysaccharides from Nelumbo nucifera Gaertn.(lotus): a review, Int. J. Biol. Macromol. 226 (2023) 562–579, https://doi.org/10.1016/j.ijbiomac.2022.12.072.
[50] H.Y. Kim, J.H. Kim, Chemical characterization of the precipitate found in and its effect on drug release of the scutellaria baicalensis-coptis chinensis extract, Chem. Biodivers. 20 (2023) e20230146, https://doi.org/10.1002/cbdv.202301461.
[51] B.F. Van Duzee, The influence of water content, chemical treatment and temperature on the rheological properties of stratum corneum, J. Invest. Dermatol. 71 (1978) 140–144, https://doi.org/10.1111/1523-1747.ep12546836.
[52] F.H. Silver, J.W. Freeman, D. DeVore, Viscoelastic properties of human skin and processed dermis, Skin Res. Technol. 7 (2001) 18–23, https://doi.org/10.1034/j.1600-0846.2001.007001018.x.
[53] K.S. Wu, W.W. Van Osdol, R.H. Dauskardt, Mechanical properties of human stratum corneum: effects of temperature, hydration, and chemical treatment, Biomaterials 27 (2006) 785–795, https://doi.org/10.1016/j.biomaterials.2005.06.019.

[54] S.N.A.M. Noor, J. Mahmud, Modelling and computation of silicone rubber deformation adapting neo-hookean constitutive equation, in: 2015 Fifth International Conference on Communication Systems and Network Technologies, IEEE, 2015, pp. 1323–1326, https://doi.org/10.1109/CSNT.2015.276.
[55] X. Kong, P. Zhou, C. Wu, Numerical simulation of microneedles' insertion into skin, Comput. Methods Biomech. Biomed. Eng. 14 (2011) 827–835, https://doi.org/10.1080/10255842.2010.497144.
[56] X. Kong, C. Wu, Measurement and prediction of insertion force for the mosquito fascicle penetrating into human skin, JBE 6 (2009) 143–152, https://doi.org/10.1016/S1672-6529(08)60111-0.
[57] S. Chandbadshah, G. Mannayee, Structural analysis and simulation of solid microneedle array for vaccine delivery applications, Mater. Today: Proc. 65 (2022) 3774–3779, https://doi.org/10.1016/j.matpr.2022.06.483.
[58] P. Su, Y. Yang, L. Huang, Biomechanical simulation of needle insertion into cornea based on distortion energy failure criterion, Acta Bioeng. Biomech. 18 (2016) 65–75, https://doi.org/10.5277/ABB-00248-2014-02.
[59] S. Shetty, Investigation of Geometrical Effects on Microneedle Reliability for Transdermal Applications, University of South Florida, 2005.
[60] Z. Faraji Rad, R.E. Nordon, C.J. Anthony, L. Bilston, P.D. Prewett, J.-Y. Arns, C.H. Arns, L. Zhang, G.J. Davies, High-fidelity replication of thermoplastic microneedles with open microfluidic channels, Microsystems & nanoengineering 3 (2017) 1–11, https://doi.org/10.1038/micronano.2017.34.
[61] A.A. Ioannides, G.K. Kostopoulos, L. Liu, P.B. Fenwick, MEG identifies dorsal medial brain activations during sleep, Neuroimage 44 (2009) 455–468, https://doi.org/10.1016/j.neuroimage.2008.09.030.
[62] M. Massimini, R. Huber, F. Ferrarelli, S. Hill, G. Tononi, The sleep slow oscillation as a traveling wave, J. Neurosci. 24 (2004) 6862–6870, https://doi.org/10.1523/jneurosci.1318-04.2004.
[63] E. Altena, Y.D. Van Der Werf, E.J. Sanz-Arigita, T.A. Voorn, S.A. Rombouts, J.P. Kuijer, E.J. Van Someren, Prefrontal hypoactivation and recovery in insomnia, Sleep 31 (2008) 1271–1276, https://doi.org/10.5665/sleep/31.9.1271.
[64] D.J. Buysse, A. Germain, M. Hall, T.H. Monk, E.A. Nofzinger, A neurobiological model of insomnia, Drug Discov. Today Dis. Model. 8 (2011) 129–137, https://doi.org/10.1016/j.ddmod.2011.07.002.
[65] S. Suh, H. Kim, T.T. Dang-Vu, E. Joo, C. Shin, Cortical thinning and altered cortico-cortical structural covariance of the default mode network in patients with persistent insomnia symptoms, Sleep 39 (2016) 161–171, https://doi.org/10.5665/sleep.5340.
[66] C. He, W. Huang, G. Zhong, H. Wu, L. Cheng, Y. Wen, J. Lin, A smart flexible sleep-aid eye mask based on acupoint electric pulse stimulation combined bioelectrical signal feedback,IEEE, Internet Things J 11 (4) (2024) 7228–7240, https://doi.org/10.1109/JIOT.2023.3315508.